Correcting Regional Seismic Discriminants

For Path Effects In Western China

H. E. Hartse, R. A. Flores*, and P. A. Johnson

Earth and Environmental Sciences Division
Los Alamos National Laboratoy
Los Alamos, New Mexico 87545

For Submission to *Bulletin of the Seismological Society of America*

June 4, 1997

LAUR-97-1978

* Now at National Center For Genome Research, Santa Fe, NM 87505

Abstract

The effect of path on regional seismic wave propagation can be significant. In an effort to improve discriminant performance, we explore the effect of path upon P_g/L_g ratios. Our primary objective is to find path corrections that reduce scatter within earthquake and explosion ratio populations, while at the same time increase the separation between the two populations. We emphasize the 1.5-3 Hz and 2-4 Hz bands, as P_g and L_g in these bands can be observed at smaller magnitudes and greater distances than higher-frequency bands, which have previously been shown to be reliable discriminants. For data we use about 270 earthquakes from northwest China and about 25 nuclear explosions from the Kazakh Test Site (KTS) recorded at station WMQ. We also use about 170 earthquakes from the same region and 7 nuclear explosions from the Lop Nor Test Site recorded at station AAK. In addition to ratio-distance trends, we examine P_g/L_g ratio-parameter trends for path effects related to topography, basin thickness, and crustal thickness. These include, roughness (RMS), mean, maximum, and minimum for each of the three path parameters, and we also examine gradient measurements for each of the three path parameters. Through linear regressions, we found path corrections that will reduce scatter within event populations, and we also found path corrections that increase the separation between earthquakes and KTS explosions recorded at WMQ. We obtained the best improvement in discrimination performance at WMQ by removing a topography roughness trend and a gradient trend of basin thickness after weighting each parameter by path length. However, for AAK we found no consistent path corrections that improve discriminant performance over the uncorrected case, probably because the paths for most of the earthquakes and explosions that we examined at AAK are quite similar. Because we see no predictable or repeatable trends for "adjacent" central Asian stations and overlapping regions of interest, we recommend an even more empirical approach to correcting for the effect of path. Where earthquakes are abundant, such as the Tian Shan, contouring a grid of ratio residuals (for each band of interest), may be a simpler method of finding appropriate path corrections.

Introduction

Monitoring the Comprehensive Test Ban Treaty (CTBT) to magnitude levels below 4.0 will require use of regional seismic data recorded at distances of less than 2000 km. Hartse *et al*. (1997) report that for the region surrounding station WMQ in northwest China, P_g/L_g ratios at frequencies greater than 3 Hz separate earthquakes from nuclear explosions. However, as magnitude drops below 4, many regional events measured in the 3-6 Hz band cannot be analyzed because signal levels fall to noise levels (Taylor and Hartse, 1996). One solution to this problem is to site new stations where noise levels are low, as has been discussed by Kim *et al*. (1996). Another solution is to use lower-frequency ($f < 3$ Hz) ratios as discriminants. That is, for $f < 3$ Hz, if the scatter within earthquake and explosion populations could be reduced, and the separation between the two populations increased, then smaller events could be identified at greater distances. One approach to reducing measurement scatter is to correct for the effect of physical parameters along the event-station path.

The effect of path on regional phase amplitudes have been widely discussed (*e.q.* Kadinsky-Cade *et al*. (1981), Gregersen (1984), and Campillo *et al*. (1993). Zhang and Lay (1994), showed that statistical trends exist between topography and some phase amplitude ratios for nuclear explosions from the Former Soviet Union's Kazakh Test Site (KTS) recorded at several seismic stations distributed throughout Eurasia. Their observations indicate that it might be possible to better discriminate nuclear events from earthquakes by correcting amplitude ratios for topographical influences. Later, Zhang *et al.* (1996) obtained a reduction in variance of earthquake phase ratios from the western United States by correcting for surface roughness. Recently, using a multivariate approach, Fan and Lay (1997) have corrected earthquake phase ratios from western China for the effects of topography, basin thickness (or sediment cover), and crustal thickness, reducing variance in the P_g/L_g measurements for frequencies less than 3 Hz by a factor of two or more relative to standard distance corrections.

While these earlier studies have shown that variance reduction within an earthquake-ratio population is possible, they do not address whether separation between earthquakes and explosions can actually be increased by correcting for path effect. In this paper we measure the change in separation between earthquake and explosion populations after correcting P_g/L_g ratios for path effects related to topography, basin thickness, and crustal thickness. For northwest China earthquakes and nuclear explosions from KTS recorded at WMQ, we find

that distance-weighted topography and distance-weighted basin thickness corrections do indeed improve the P_g/L_g discriminant for the 1.5-3 and 2-4 Hz bands. We speculate that this increased separation occurs because the explosions from KTS traverse paths with relatively smooth topography and uniform crustal thickness, while most earthquakes we studied have more complicated paths, traversing the topographically rough Tian Shan, the Tarim Basin, and the Junggar Basin. For northwest China earthquakes and nuclear explosions from the Lop Nor test site recorded at AAK, we do not find path corrections that improve the P_g/L_g discriminant. We speculate that this is because the Lop Nor explosions and most of the earthquakes studies at AAK traverse similar paths that include thick sediments of the Tarim Basin and rough topography along the Tian Shan. Below, we describe our data and analysis methods. Then we describe results and provide a short discussion.

Data and Method

We selected waveforms recorded at WMQ in northwest China and AAK in Kyrgyzstan because these are the longest continuously operating stations in the region, and because a detailed discrimination study using these stations has been conducted by Hartse *et al.* (1997). WMQ was upgraded to a digital broadband station in late 1986 and AAK became operational in 1990. WMQ has recorded over 25 KTS explosions (at a distance of about 960 km) and regional earthquakes. AAK has recorded 7 Lop Nor nuclear explosions (at a distance of about 1190 km) and many regional earthquakes. We obtained event locations (Figure 1), magnitudes, and origin times from United States Geological Survey Preliminary Determination of Epicenter (PDE) catalogs for the years 1987-1996 (Gao and Richards, 1994), and we obtained event information from regional Chinese catalogs for earthquakes smaller than about magnitude 4.0 for the years 1987-1989. Event magnitudes for the complete data set range between 2.5 and 6.2 for the earthquakes and 4.5 and 6.5 for the nuclear explosions. A more detailed discussion of the data set is available in Hartse *et al.* (1997).

The path parameters that we studied are topography (Figure 1), basin thickness (or depth to basement) (Figure 2), and crustal thickness (or depth to moho) (Figure 3). We obtained all path data from the Cornell Geophysical/Geological Information and Data Server for Eurasia (Fielding *et al.*, 1993). These include the ETOPO5 topography data set, and the depth to moho and depth to basement data sets from the Institute for Physics of the Earth (Moscow). The horizontal resolution of the data sets is ≈ 10 km. While this is rather coarse resolution,

and in the case of basin thickness and crustal thickness there are surely inaccuracies, these data sets do provide a basis for measuring large-scale trends. Sample cross sections for a KTS explosion recorded at WMQ are shown in Figure 4. Map views of the line of cross section are indicated on Figures 1, 2, and 3.

For this study we have concentrated on P_g/L_g phase ratios, testing overlapping, one-octave bands ranging from 0.75-1.5 Hz up through 3-6 Hz. We chose the P_g/L_g ratios because they have shown promise as a globally transportable discriminant (Walter *et al*. (1995), Hartse *et al*. (1997)). Our first processing step is to form P_g/L_g amplitude ratios. After bandpass filtering, we measured the RMS amplitude (in the Log_{10} domain) for P_g, L_g, and pre-event noise. Measurement windows are defined by velocities (6.2 to 5.2 km s^{-1} for P_g and 3.6 to 3.0 km s^{-1} for L_g) and epicentral distance. We required both phases to have signal level that exceeded pre-event noise level by a factor of 2 before forming a ratio. Using these ratios and the event magnitudes we formed "uncorrected" discrimination plots such as in Figure 5.

Next, we experimented with several different path corrections. These are simple regressions of the uncorrected ratio versus the parameter of interest. For each regression, we use only the uncorrected earthquake ratios that have signal level at least five times the pre-event noise level. When we remove a trend from the data we use all earthquake and explosion ratios formed. A common path correction used by many researchers is the distance correction (Figure 6). We find the linear trend of ratio versus distance within the earthquake population, and then remove the trend from the earthquake and the explosion populations to produce a corrected-ratio versus magnitude plot (Figure 6). In our example, the P_g/L_g (2-4 Hz) ratio has a positive trend with distance. Hence, upon removal of the the trend, the distant KTS explosions are actually pulled closer to the earthquake population, even though the scatter within the earthquakes is reduced.

For topography, basin thickness, and crustal thickness, we followed Zhang and Lay (1994). and experimented with several variations of these physical parameters. For each of these three basic parameters, we projected the great circle connecting an epicenter to the station through a parameter grid as shown for the path KTS to WMQ in Figure 1, 2, and 3. We extracted a parameter value every 10 km along each path, and then reduced the multiple measurements from each path into a single statistical value. For each path we found the maximum, minimum, and mean value. The mean $\bar{(x)}$ is defined by

$$\bar{x} = \frac{1}{N} \sum_{i=1}^{N} x_i \,, \tag{1}$$

where N is the total number of samples, and x_i the measurement taken at the i^{th} position along the path. Another statistical value we considered, root mean square roughness along a path, is defined as

$$RMS\ \ roughness = \sqrt{\frac{1}{N} \sum_{i=1}^{N} (x_i - \bar{x})^2}. \tag{2}$$

This is a measure of how widely the parameter varies along a given path. We also considered how the gradients of topography, basin thickness, and crustal thickness vary along each path. We define gradient as

$$gradient = \frac{(x_{i+1} - x_i)}{\tau_0} \,, \tag{3}$$

where τ_0 is the sample spacing along the path. There are $N-1$ gradient values along each path, and we reduced these gradient values to the single measurements of maximum gradient, minimum gradient, mean gradient, and RMS gradient for a given path. Thus, when the reduced parameter values and the reduced gradient values are considered together, we tested 8 path values (maximum, minimum, mean, RMS, gradient maximum, gradient minimum, gradient mean, and gradient RMS) that are each associated with topography, basin thickness, and crustal thickness.

As in the case for the distance correction, we plotted each path measurement versus the discriminant ratio, and we applied a linear regression to the earthquake data. Figure 7 is an example of correcting the P_g/L_g (2-4) Hz ratio for the path effect of topographic roughness (TOPO RMS). This is a weak trend, which when removed, slightly reduces the earthquake scatter and slightly increases separation between the explosions and the earthquakes compared to the uncorrected case shown in Figure 5.

Following Zhang *et al.* (1996), we experimented with weighting path parameters by multiplying by path length. The idea behind this approach is that a long path with some set of physical characteristics, should effect phase amplitudes more than a short path with the same physical characteristics. Figure 8 is an example where we weighted the topographic roughness by the path distance. Removing this trend from the phase ratios reduces scatter within the earthquake population and increases the separation between the earthquake and explosion

populations.

To quantify the improvement (or degradation) in discriminant performance for each correction, we calculate the Mahalonobis Distance, Δ^2 a measure that depends on scatter within each population and the separation between the population means,

$$\Delta^2 = \frac{(\bar{v_x} - \bar{v_q})^2}{\sigma_x^2 + \sigma_q^2}, \tag{4}$$

where $\bar{v_x}$ is the mean of the explosion ratios, $\bar{v_q}$ is the mean of the earthquake ratios, σ_x^2 is the variance of the explosion ratios, and σ_q^2 is the variance of the earthquake ratios. Note that the Mahalonobis Distance is posted on each ratio-magnitude discrimination plot in Figures 5, 6, 7, and 8.

Results and Discussion

We tested several path corrections for P_g/L_g bands from 0.75-1.5 Hz up to 3-6 Hz, experimenting with mean, maximum, minimum, and RMS, of topography, basin thickness, and crustal thickness, and we also experimented with mean, maximum, minimum, and RMS of the gradient of each path parameter. In addition, we also experimented by weighting each path value by path length. In general, we found that for many corrections, the scatter within the earthquake population can be reduced, but this does not necessarily increase the separation between the earthquakes and explosions, nor does it increase the Mahalonobis Distance. The most consistent example where a correction reduces scatter within the earthquake population while also reducing separation between populations is for distance (Figure 6). That is, although scatter within the earthquake population is reduced, KTS explosion ratios are pulled closer to the earthquakes by removing the distance trend.

we are especially interested in improving the relatively low-frequency P_g/L_g discriminants (such as 1.5-3 Hz and 2-4 Hz), as these bands can be applied at greater distance and lower magnitude than higher-frequency bands. Figure 9 presents results for several parameter tests of the RMS value for the 2-4 Hz P_g/L_g band at WMQ. To keep the plot relatively simple, we show only RMS results, but plots for mean, maximum, and minimum are similar. For WMQ we find that removing the TOPO RMS or BASM RMS trend improves separation between earthquakes and KTS explosions slightly over the uncorrected case. Even better improvement is obtained by removing the trend of TOPO RMS that has been weighted by distance. Note, however, that distance weighting can also degrade the separation for some

parameters. For instance, separation after removing the BASM RMS trend increases relative to the uncorrected case, but weighting by path length (DIST x BASM RMS) reduces Mahalonobis Distance from 6.3 (for the uncorrected) case to 5.4.

Overall, the corrections that improved separation (relative to the uncorrected case) the most are DIST x TOPO RMS and DIST x BASM GRMS. Also, for WMQ we find that a correction that improves separation for a given P_g/L_g band, will generally improve separation for all the P_g/L_g bands that we considered (Figure 10). For example, the DIST x BASM GRMS increases Mahalonobis Distance for the 1-2 Hz band and all higher bands relative to the respective uncorrected case.

For AAK we could not find any parameter correction that consistently improves performance over the uncorrected case (Figure 11). A few corrections do increase Mahalonobis Distance slightly for a few bands. For example, the roughness of the crustal thickness (MOHO RMS) improves the P_g/L_g 1.5-3 Hz and 2-4 Hz discriminants slightly over the uncorrected case, but slightly degrades the 1-2 Hz and 3-6 Hz discriminants (Figure 11). The paths for many of the earthquakes and for the Lop Nor explosions that we evaluated at AAK are quite similar. Many paths traverse rough topography of the Tian Shan and cross the northern Tarim Basin (Figures 1 and 2). Hence, scatter within populations can be reduced, but separation between populations is not improved. On the other hand, KTS explosions recorded at WMQ traverse gentle topography relative to most northwest China earthquakes. Also, many of the earthquakes cross portions of the Tarim Basin and also the Junggar Basin, while KTS explosions cross only the Junggar Basin. Thus, it appears that improvement in discriminant performance is possible when the explosions have unique path features relative to earthquakes.

We feel that our study demonstrates a few problems with removing the effect of path from amplitude ratios. We have not been able to find common trends at AAK and WMQ that actually improve discriminant performance. We have been able to find a few trends that highlight some unique characteristics of the KTS to WMQ path relative to most other paths in the study area (DIST x TOPO RMS and DIST x BASM GRMS). These trends are not unique to the Lop Nor to AAK path, and hence do not improve P_g/L_g discriminants at AAK. Indeed, it appears that there are many more parameter trends available that actually degrade discriminant performance rather than improve performance. Even if we do a multivariate regression, examining several parameters simultaneously in an attempt to reduce ratio scatter (Fan and Lay, 1997), we suspect that the path parameters (and the parameter coefficients)

selected by such an analysis will vary widely between stations from the same region (such as the case of AAK and WMQ).

We suggest an even more empirical approach, relying solely on the amplitudes of the observed data. Ratio residuals for a single station and band of interest could be smoothed and gridded on a regional base map. Such a grid of ratio "corrections" could then be referenced before constructing final discrimination plots. We are currently investigating this approach and will report on results in a later paper. The primary drawback to this empirical method will be that it will only be possible for regions of relatively high seismicity.

Summary and Conclusions

Using stations WMQ in northwest China and AAK in Kyrgyzstan, we have investigated the effect of path on the P_g/L_g seismic discriminant. Physical parameters we considered are topography, basin thickness, and crustal thickness. We measured P_g/L_g ratios from several hundred northwest China earthquakes and about 32 nuclear explosions in frequency bands ranging from 0.75-1.5 Hz to 3-6 Hz. Our primary objective was to find path corrections that would reduce scatter within earthquake and explosion populations, while at the same time increase the separation between the two populations. Through linear regressions, we found many path corrections that will reduce scatter within event populations. We also found path corrections that increase the separation between earthquakes and KTS explosions recorded at WMQ. We obtained the best improvement in discrimination performance by removing a topography roughness trend and a gradient of basin thickness trend from the data after weighting each path's measurement by distance. The best discriminant improvement we obtained for path parameters that were not weighted by distance was by removing the trend for topography roughness. However, for Lop Nor explosions and earthquakes recorded at AAK, we found no parameter trends that could be exploited to consistently improve discriminant performance, probably because these earthquake and explosion paths are so similar. Rather than searching for specific path parameters, which may or may not improve discriminant performance, we suggest that for regions such as northwest China, where natural seismicity is high, empirical corrections should be derived from the residuals of the observed earthquake ratios.

Acknowledgements

We thank Steve Taylor and two anonymous reviewers for thoughtful comments, and Scott Phillips for retrieving WMQ waveforms. We thank the staff at the IRIS Data Management Center for prompt replies to our data requests. Maps and cross-sections were created using using the Global Mapping Tool (GMT) (Wessel and Smith, 1991). This work is in support of the DOE Comprehensive Test Ban Treaty Research and Development Program, ST482A, and was performed at Los Alamos National Laboratory under the auspices of the United States Department of Energy, Contract Number W-7405-ENG-36.

Hans E. Hartse telephone: 505-665-8495 email: hartse@lanl.gov
Geophysics Group, EES-3 fax: 505-667-4739
Earth and Environmental Sciences Division
Los Alamos National Laboratory
Los Alamos, NM 87545

References

Campillo, M., B. Feignier, M. Bouchon, and N. Bethoux (1993). Attentuation of crustal waves across the Alpine Range, *J. Geophys. Res.*, **98**, 1987-1996.

Fan, G. and T. Lay (1997). Statistical analysis of irregualr waveguide influences on regional seismic discriminants in China, *Bull. Seis. Soc. Am.*, **87**, xx-yy.

Fielding, E. J., M. Barazangi, and B. L. Isacks (1993). A geological and geophysical data base for Eurasia, *Final Technical Report, ARPA NMRO F29601-91-K-DB08*, xx-yy.

Gao, L. and P. G. Richards (1994). Studies of earthquakes on and near the Lop Nor, China, nuclear test site, *Proceedings of the 16th Annual DARPA/AF Seismic Research Symposium*, 106-112.

Gregersen, S. (1984). L_g wave propagation and crustal structure differences near Denmark and the North Sea, *Geophys. J. R. astr. Soc.*, **79**, 217-234.

Hartse, H. E., S. R. Taylor, W. S. Phillips, and G. E. Randall (1997). Preliminary study of seismic discrimination in central Asia with emphasis on western China, *Bull. Seis. Soc. Am.*, **87**, 1464-1474.

Kadinsky-Cade, K. M., M. Barazangi, J. Oliver, and B. Isacks (1981). Lateral variations of high-frequency seismic wave propagation at regional distances across the Turkish and Iranian Plateaus, *J. Geophys. Res.*, **86**, 9377-9396.

Kim, W-. Y., V. Aharonian, A. L. Lerner-Lam, and P. G. Richards (1996). Discrimination of earthquakes and explosions in Southern Russian using regional high-frequency three-component data from the IRIS/JSP Caucasus network, *Bull. Seism. Soc. Am.*, **86**, in.

Taylor, S. R. and H. E. Hartse (1996). Regional phase seismic detection thresholds at WMQ, Los Alamos National Laboratory, LAUR-96395, 6pp.

Walter, W. R., K. M. Mayeda, and H. J. Patton (1995). Phase and spectral ratio discrimination between NTS earthquakes and explosions. Part I: Empirical Observations, *Bull. Seism. Soc. Am.*, **85**, 1050-1067.

Wessel, P. and W. H. F. Smith (1991). Free software helps map and display data, *EOS Trans. AGU*, **72**, 441.

Zhang, T. and T. Lay (1994a). Analysis of short-period regional phase path effects associated with topography in Eurasia, *Bull. Seis. Soc. Am.*, **84**, 119-132.

Zhang, T., T. Lay, S. Schwartz, and W. R. Walter (1996). Variation of regional seismic discriminants with surface topographic roughness in the western United States, *Bull. Seis. Soc. Am.*, **86**, 714-725.

Figure Captions

Figure 1. Shaded topography map of the study area. Nuclear explosions and earthquakes used in this study were recorded at WMQ, AAK, or at both stations. The cross section from the Kazakh Test Site (KTS) to WMQ is shown in Figure 4.

Figure 2. Shaded basin thickness (depth to basement) map of the study area. The cross section from KTS to WMQ is shown in Figure 4.

Figure 3. Shaded crustal thickness (depth to moho) map of the study area. The cross section from KTS to WMQ is shown in Figure 4.

Figure 4. Cross sections of topography, basin thickness, and crustal thickness along a line from KTS to WMQ (see Figures 1, 2, and 3). Note that vertical scales vary between cross sections.

Figure 5. An "uncorrected" P_g/L_g (2-4 Hz) discrimination plot for station WMQ. Open circles indicate regional earthquakes and asterisks indicate nuclear explosions. All explosions recorded at WMQ are from KTS, except for the smallest explosion (m_b = 4.5), which is from Lop Nor.

Figure 6. The ratio-distance trend for the P_g/L_g ratio in the 2-4 Hz band at WMQ (solid line) and the ratio-magnitude discrimination plot after the trend has been removed from the earthquakes and the explosions. Note that only earthquakes are used to find the trend. While reducing the scatter within the earthquake ratios, this correction actually creates more overlap between the explosions and earthquakes compared to the uncorrected case shown in Figure 5. Distance units are in km.

Figure 7. The ratio-topographic roughness (RMS) trend for the P_g/L_g ratio in the 2-4 Hz band at WMQ (solid line) and the ratio-magnitude discrimination plot after the trend has been removed from the earthquakes and the explosions. This is a weak trend which leaves the discrimination plot nearly unchanged compared to the uncorrected plot in Figure 5. TOPO RMS units are in km.

Figure 8. The ratio versus the distance-weighted roughness (RMS) of the basin thickness gradient (see Equation 4) for the P_g/L_g ratio in the 2-4 Hz band at WMQ (solid line) and the ratio-magnitude discrimination plot after the trend has been removed from the earthquakes and the explosions. This is a strong trend which increases the separation between KTS explosions and regional earthquakes compared to the uncorrected plot in Figure 5.

DIST TOPO RMS units are in km^2.

Figure 9. Summary discrimination plot for P_g/L_g ratio in the 2-4 Hz band at WMQ for various parameter corrections. The number posted below the error bars is the Mahalonobis Distance (Equation 5). The larger the number, the better the separation between the earthquakes and the nuclear explosions. The most successful corrections are distance-weighted roughness of the basin thickness gradient (DIST x BASM GRMS) and the distance-weighted roughness of the topography (DIST x TOPO RMS).

Figure 10. Summary discrimination plot for P_g/L_g ratios at WMQ for various parameter corrections. Bands tested are indicated along the vertical axis. The size of each square is scaled to the Mahalonobis Distance (Equation 5). Actual values range from 0.03 to 14.6. The most successful corrections are distance-weighted roughness of the basin thickness gradient (DIST x BASM GRMS) and the distance-weighted roughness of the topography (DIST x TOPO RMS).

Figure 11. Summary discrimination plot for P_g/L_g ratios at AAK for various parameter corrections. Bands tested are indicated along the vertical axis. The size of each square is scaled to the Mahalonobis Distance (Equation 5). Actual values range from 0.5 to 12.9. For AAK we found no corrections which increase Mahalonobis Distance relative to the uncorrected case.

Figure 1

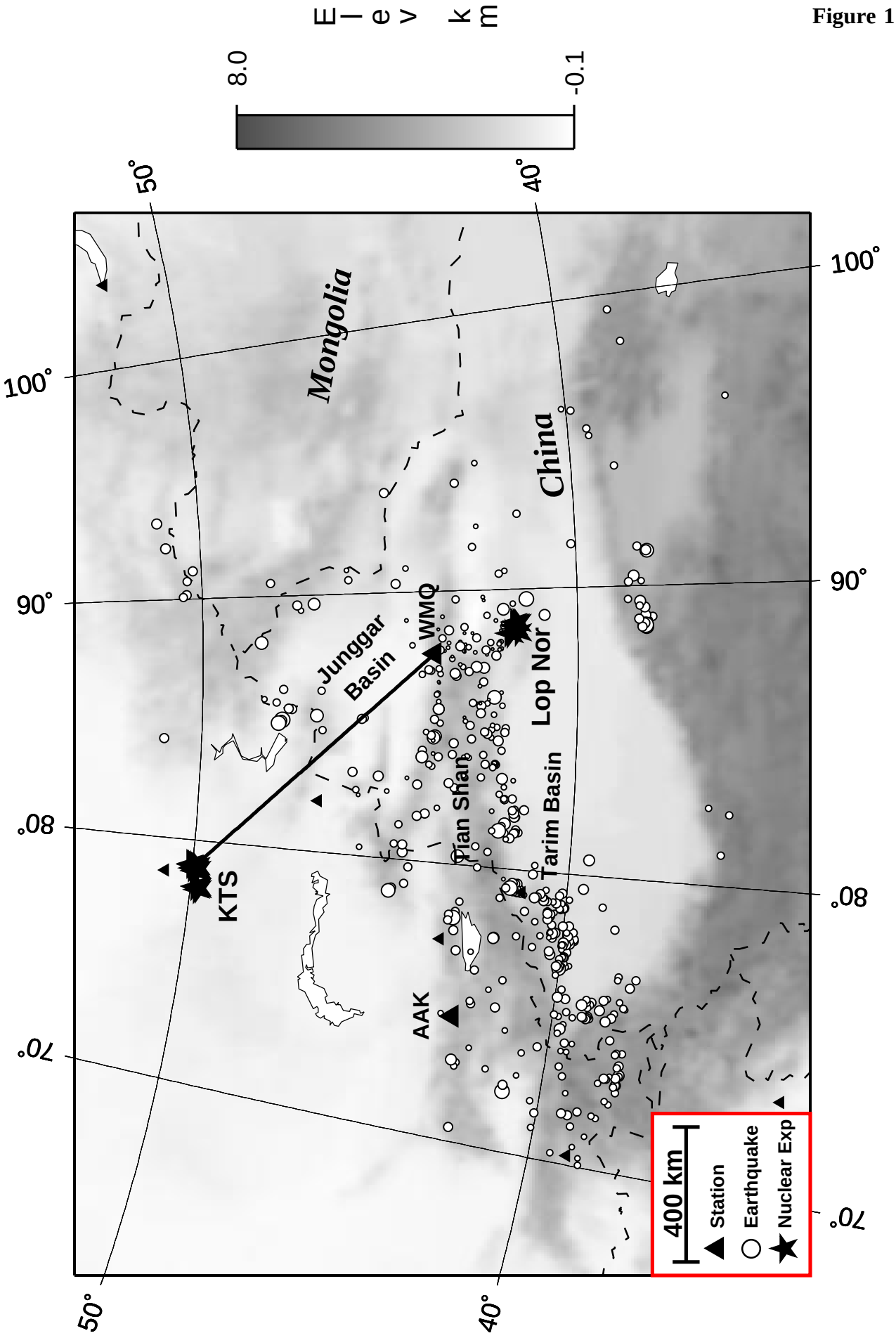
Elev km
8.0
-0.1
50°
40°
100°
90°
80°
70°
Mongolia
China
Junggar Basin
WMQ
Lop Nor
Tian Shan
Tarim Basin
KTS
AAK
400 km
Station
Earthquake
Nuclear Exp

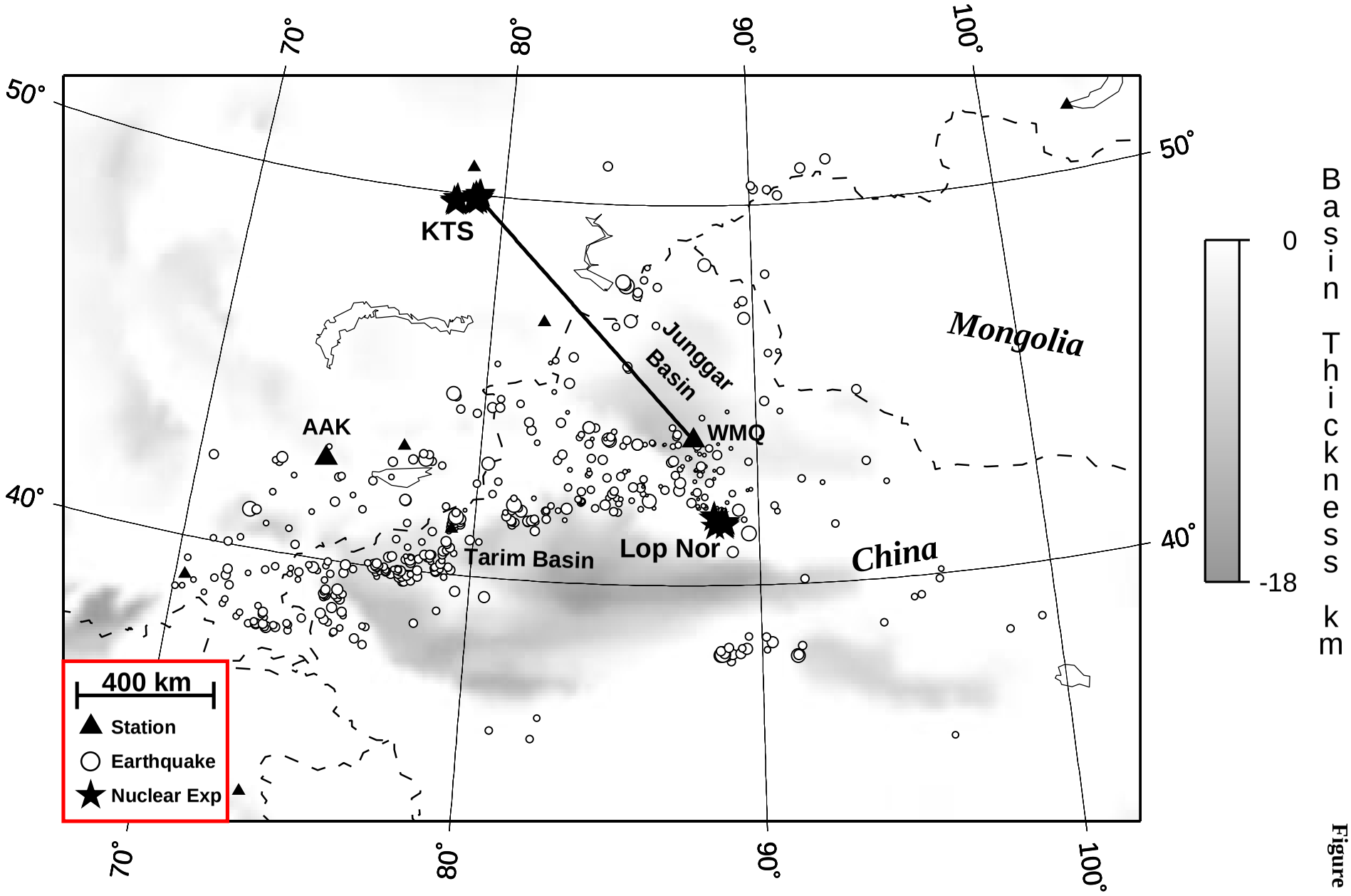
70°
80°
90°
100°
50°
40°
KTS
AAK
WMQ
Junggar Basin
Mongolia
China
Tarim Basin
Lop Nor
400 km
Station
Earthquake
Nuclear Exp
0
-18
Basin Thickness km

Figure 2

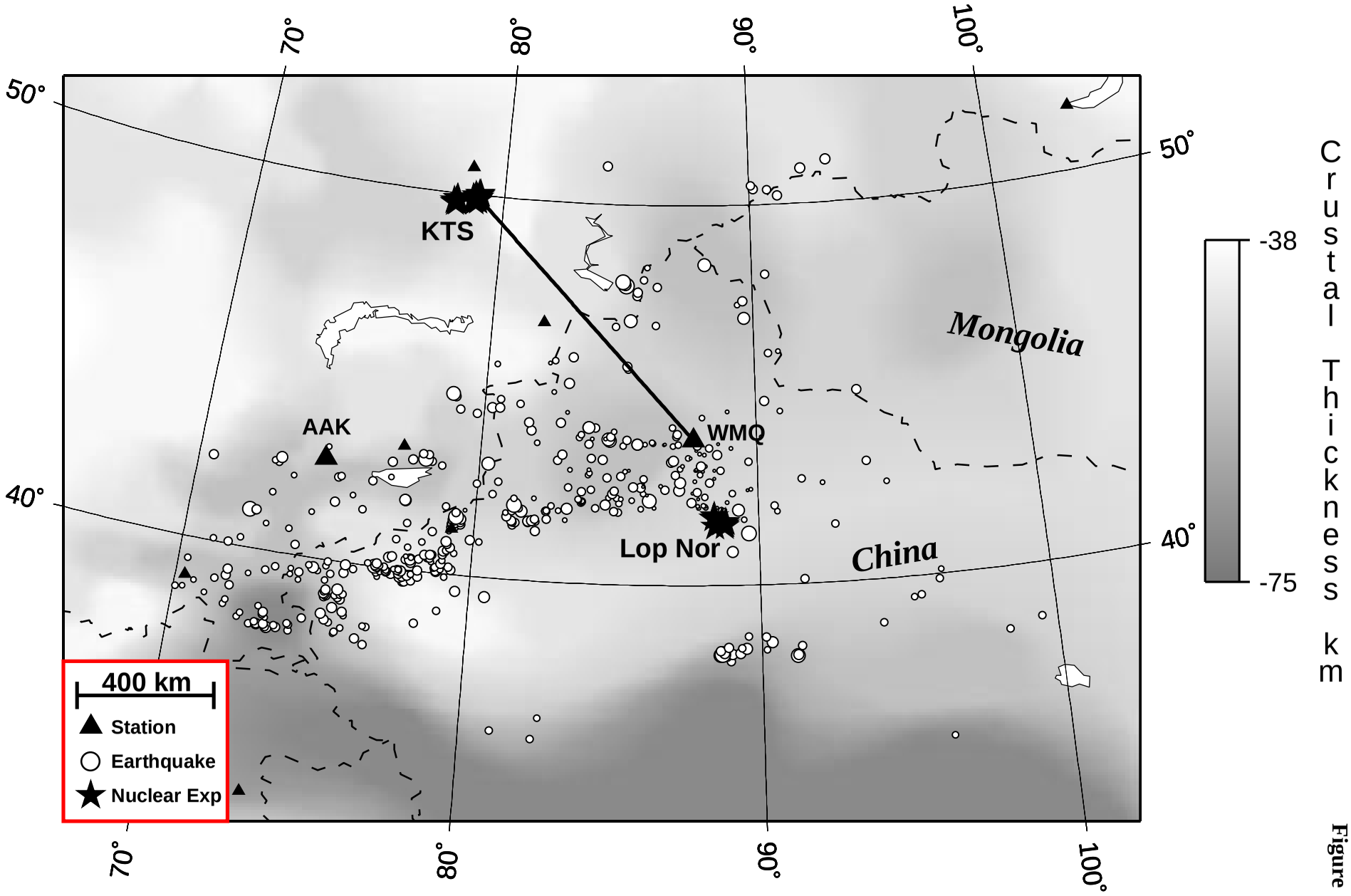
70°
80°
90°
100°
50°
40°
KTS
WMQ
AAK
Lop Nor
Mongolia
China
400 km
Station
Earthquake
Nuclear Exp
-38
-75
Crustal Thickness km

Figure 3

Figure 4

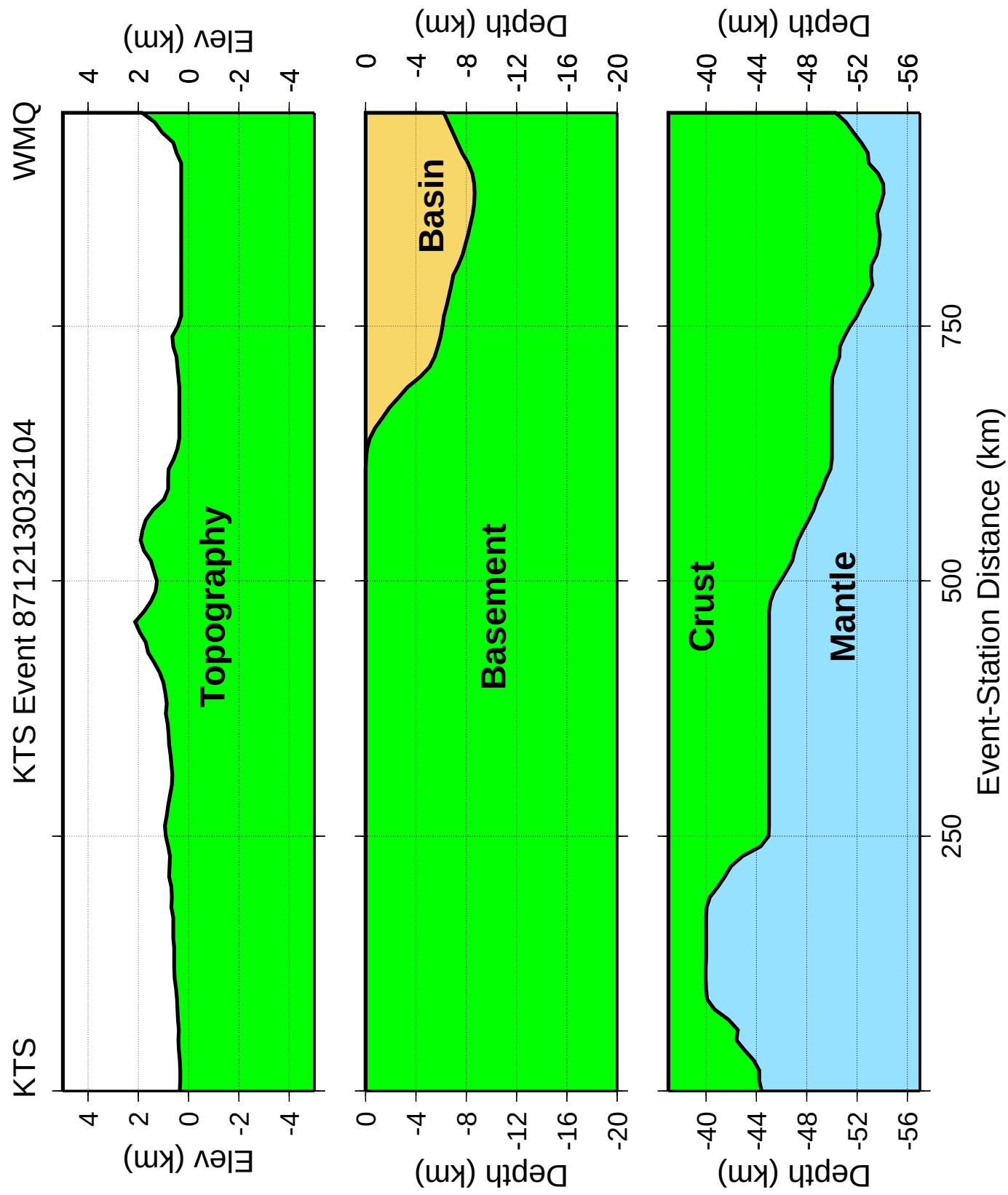
KTS
KTS Event 87121303210 4
WMQ
Elev (km)
4
2
0
-2
-4
Topography
Depth (km)
0
-4
-8
-12
-16
-20
Basin
Basement
Depth (km)
-40
-44
-48
-52
-56
Crust
Mantle
250
500
750
Event-Station Distance (km)

Figure 5

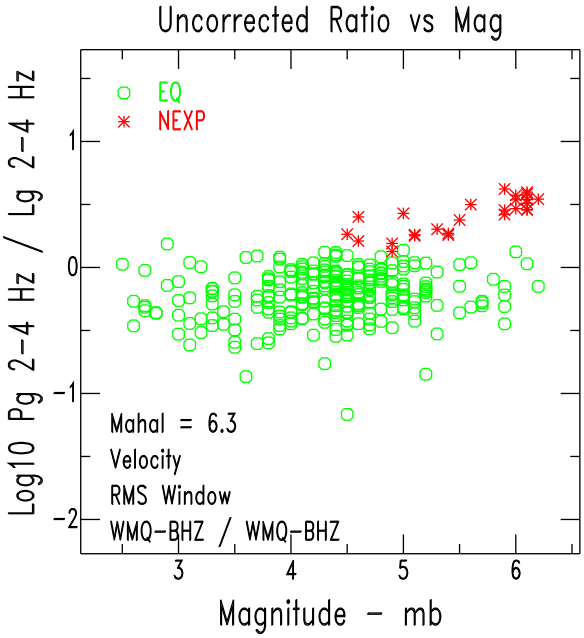
Uncorrected Ratio vs Mag
EQ
NEXP
Mahal = 6.3
Velocity
RMS Window
WMQ-BHZ / WMQ-BHZ
Log10 Pg 2-4 Hz / Lg 2-4 Hz
Magnitude - mb
1
0
-1
-2
3
4
5
6

Figure 6

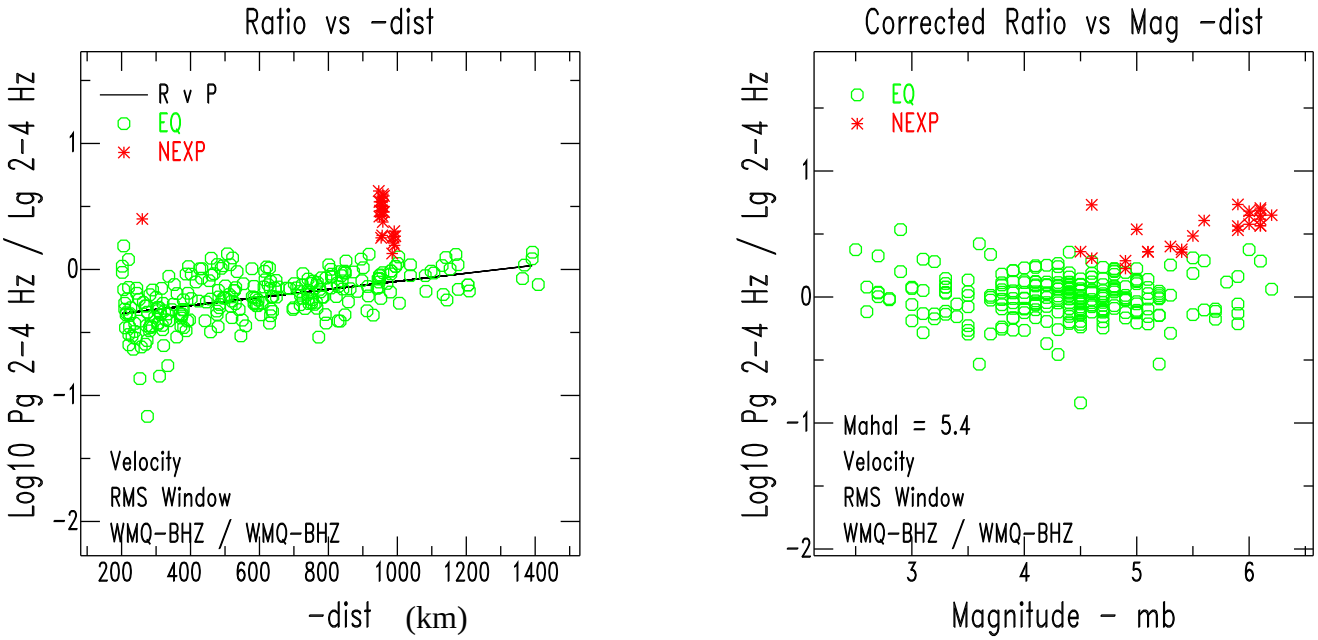
Ratio vs -dist
R v P
EQ
NEXP
Velocity
RMS Window
WMQ-BHZ / WMQ-BHZ
Log10 Pg 2-4 Hz / Lg 2-4 Hz
-dist (km)
Corrected Ratio vs Mag -dist
EQ
NEXP
Mahal = 5.4
Velocity
RMS Window
WMQ-BHZ / WMQ-BHZ
Log10 Pg 2-4 Hz / Lg 2-4 Hz
Magnitude - mb

Figure 7

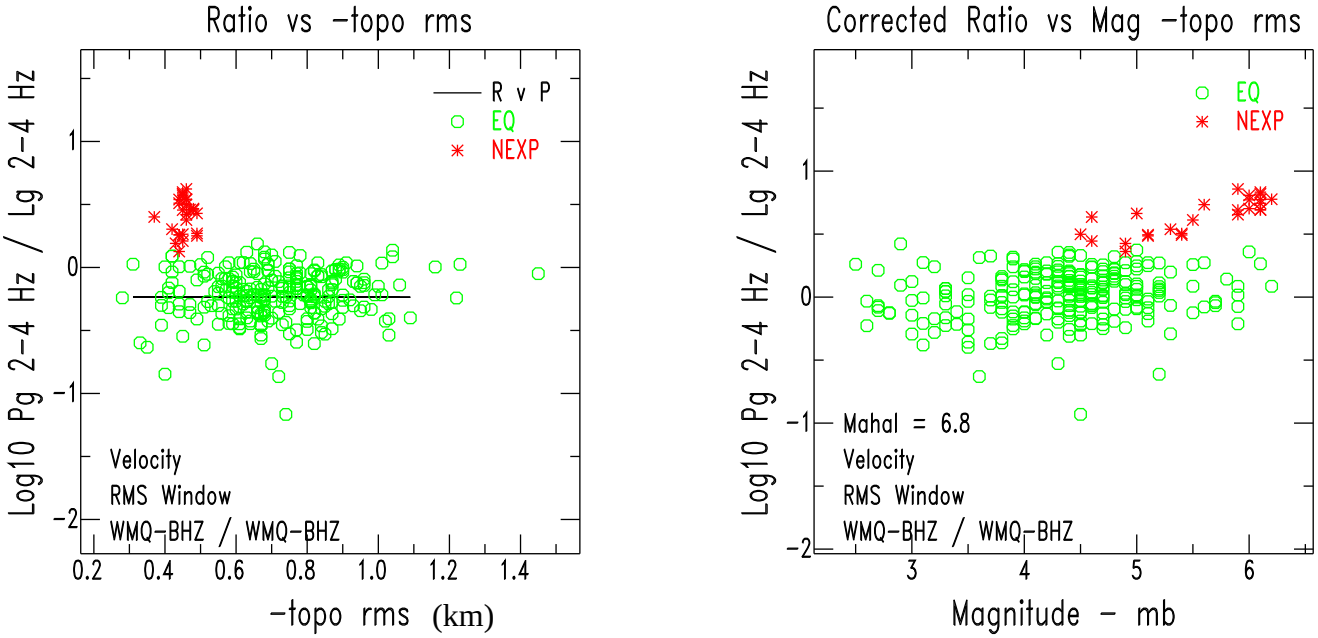
Ratio vs -topo rms
Log10 Pg 2-4 Hz / Lg 2-4 Hz
-topo rms (km)
R v P
EQ
NEXP
Velocity
RMS Window
WMQ-BHZ / WMQ-BHZ
Corrected Ratio vs Mag -topo rms
Log10 Pg 2-4 Hz / Lg 2-4 Hz
Magnitude - mb
EQ
NEXP
Mahal = 6.8
Velocity
RMS Window
WMQ-BHZ / WMQ-BHZ

Figure 8

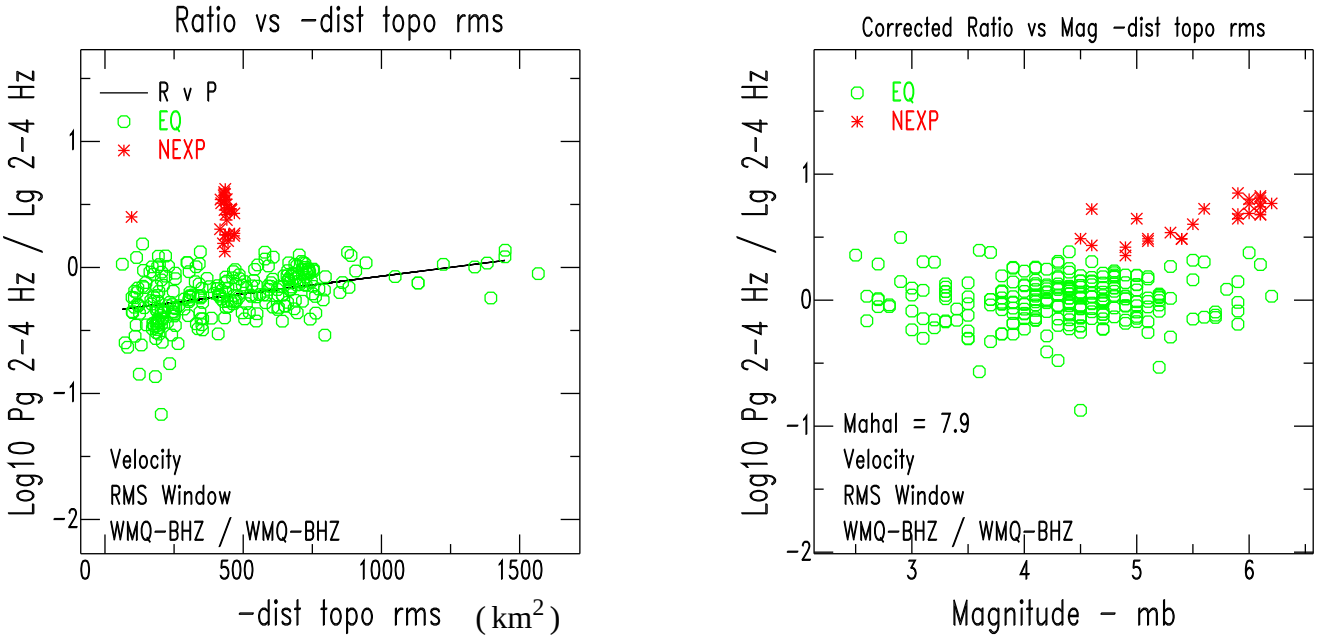
Ratio vs -dist topo rms
R v P
EQ
NEXP
Velocity
RMS Window
WMQ-BHZ / WMQ-BHZ
Log10 Pg 2-4 Hz / Lg 2-4 Hz
-dist topo rms (km²)
Corrected Ratio vs Mag -dist topo rms
EQ
NEXP
Mahal = 7.9
Velocity
RMS Window
WMQ-BHZ / WMQ-BHZ
Log10 Pg 2-4 Hz / Lg 2-4 Hz
Magnitude - mb

Figure 9

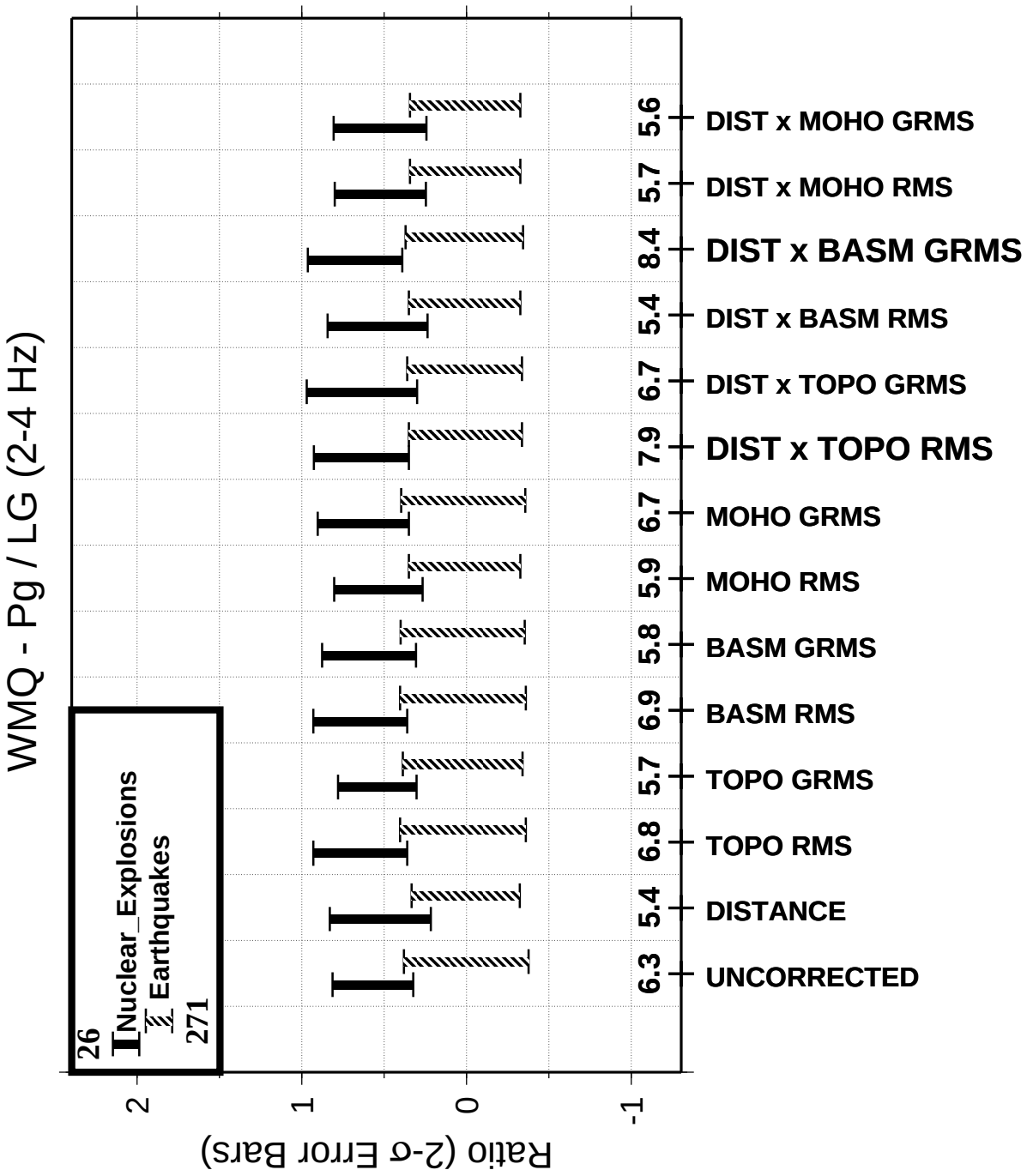
WMQ - Pg / LG (2-4 Hz)
Ratio (2-σ Error Bars)
2
1
0
-1
26
Nuclear_Explosions
Earthquakes
271
6.3
UNCORRECTED
5.4
DISTANCE
6.8
TOPO RMS
5.7
TOPO GRMS
6.9
BASM RMS
5.8
BASM GRMS
5.9
MOHO RMS
6.7
MOHO GRMS
7.9
DIST x TOPO RMS
6.7
DIST x TOPO GRMS
5.4
DIST x BASM RMS
8.4
DIST x BASM GRMS
5.7
DIST x MOHO RMS
5.6
DIST x MOHO GRMS

Figure 10

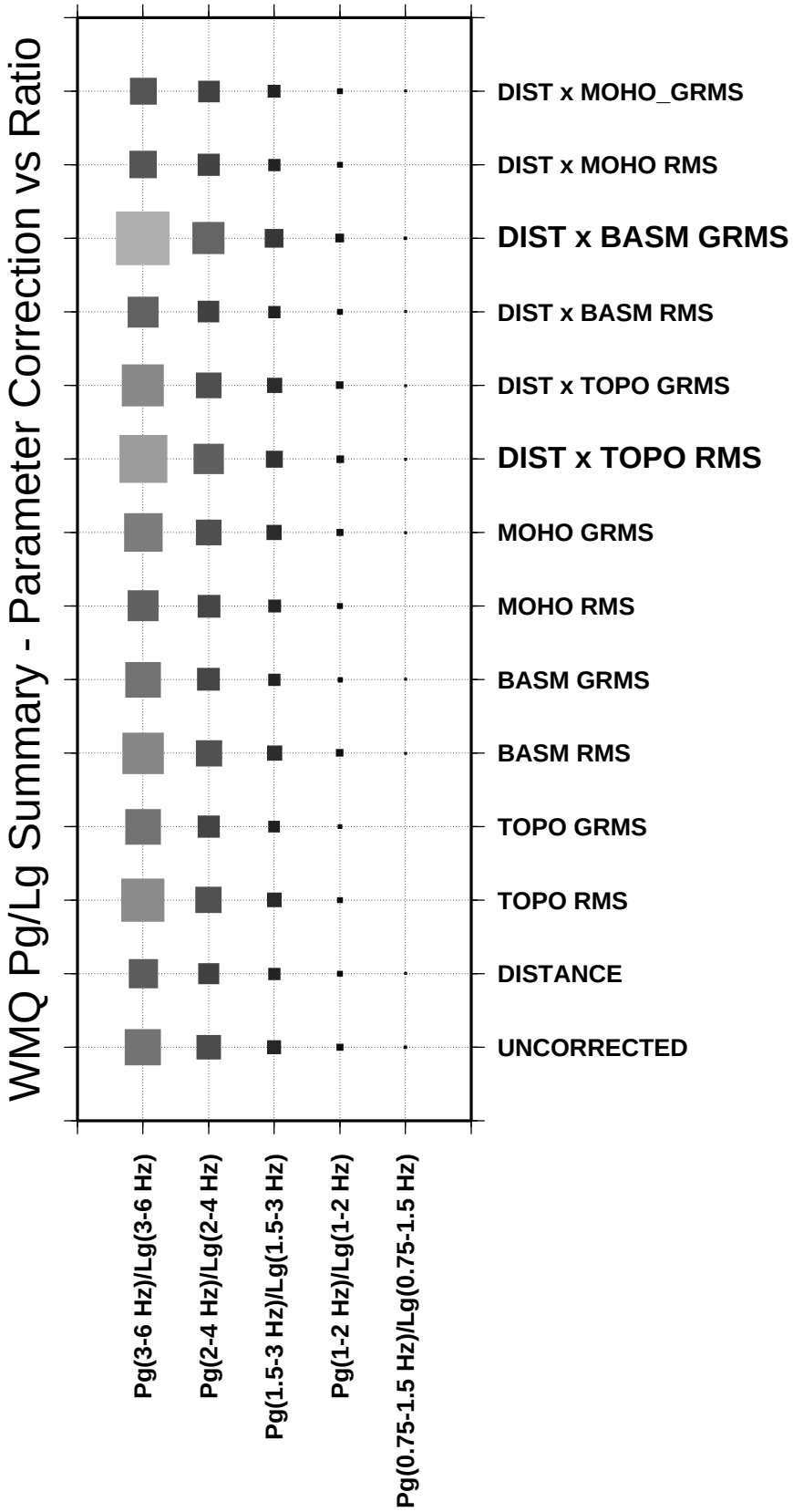
WMQ Pg/Lg Summary - Parameter Correction vs Ratio
DIST x MOHO_GRMS
DIST x MOHO RMS
DIST x BASM GRMS
DIST x BASM RMS
DIST x TOPO GRMS
DIST x TOPO RMS
MOHO GRMS
MOHO RMS
BASM GRMS
BASM RMS
TOPO GRMS
TOPO RMS
DISTANCE
UNCORRECTED
Pg(3-6 Hz)/Lg(3-6 Hz)
Pg(2-4 Hz)/Lg(2-4 Hz)
Pg(1.5-3 Hz)/Lg(1.5-3 Hz)
Pg(1-2 Hz)/Lg(1-2 Hz)
Pg(0.75-1.5 Hz)/Lg(0.75-1.5 Hz)

Figure 11

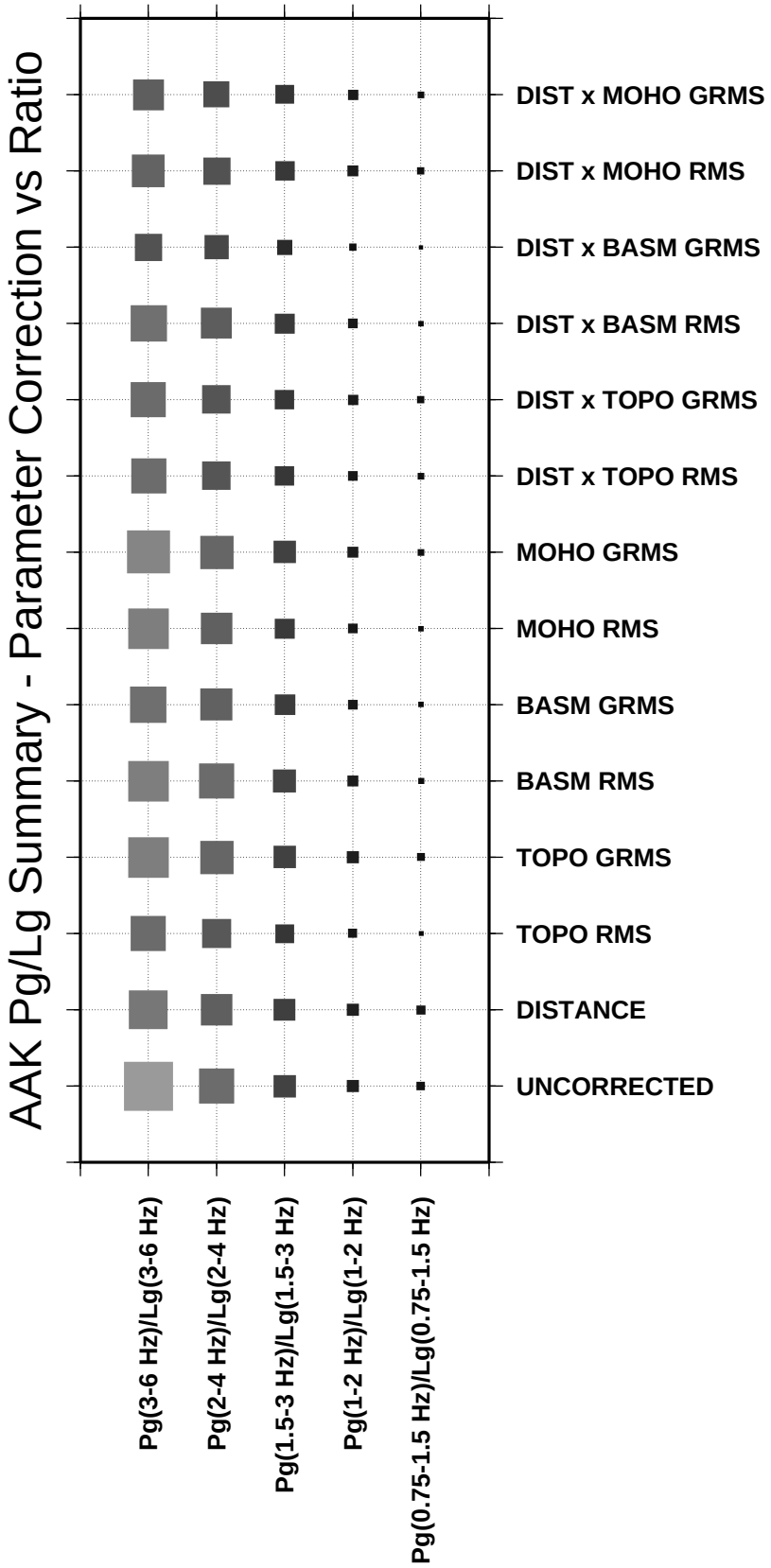
AAK Pg/Lg Summary - Parameter Correction vs Ratio
DIST x MOHO GRMS
DIST x MOHO RMS
DIST x BASM GRMS
DIST x BASM RMS
DIST x TOPO GRMS
DIST x TOPO RMS
MOHO GRMS
MOHO RMS
BASM GRMS
BASM RMS
TOPO GRMS
TOPO RMS
DISTANCE
UNCORRECTED
Pg(3-6 Hz)/Lg(3-6 Hz)
Pg(2-4 Hz)/Lg(2-4 Hz)
Pg(1.5-3 Hz)/Lg(1.5-3 Hz)
Pg(1-2 Hz)/Lg(1-2 Hz)
Pg(0.75-1.5 Hz)/Lg(0.75-1.5 Hz)